Nonreciprocal Intelligent Soundproof Barrier with Active Nonlocal Acoustic Metastructure

Yue Zhuo, Xue Chen, Ziling Liu, Zong-Qiang Sheng, and Hong-Wei Wu**

Sound insulation is an important issue in daily life and has applications in various scenarios. Conventional acoustic passive metamaterial barriers are designed as a reciprocal sound insulation. However, for some specific application scenarios, unidirectional acoustic insulation is required, which is an enormous challenge for breaking the reciprocity of sound transport with conventional passive metamaterials. Here, a soundproof barrier with nonlocal acoustic metastructure is proposed, which consists of a microcontroller to connect a pair of spatially separated microphones and speakers, to tailoring the acoustic wave transmission for realizing nonreciprocal acoustic insulation. The theoretical calculation and experiment measurement indicated that the active acoustic barrier with a selectable working frequency can realize the suppressive effect in one direction and the enhancive effect in the other direction for an incident acoustic signal. Particularly, the function of an active soundproof barrier can be freely switched to forward, backward, and bidirectional sound insulation by tailoring the nonlocal distance of the digital meta-atom. Furthermore, this acoustic metastructure is extended from a one-dimentional waveguide to a two-dimentional plane to illustrate that it is still valid in an open-field environment. The proposed customizable nonreciprocal soundproof barriers provide an avenue for many applications in the specific scenarios that require unidirectional sound insulation and high air permeability.

1. Introduction

Sound insulation or noise attenuation is a crucially important topic in the acoustic field and have many applications in several scenarios, such as heavy machinery cabins, buildings, and stations. Simultaneously, the high ventilation be also required for practical applications. However, it is incompatible between sound-insulating efficiency and ventilating capability for conventional acoustic barriers.[1,2] With the development of acoustic metasurface, it becomes possible to design soundproof barriers to realize efficient sound insulation and ventilation simultaneously.[3] In past decay, various localized subwavelength resonant units have been designed to construct the metasurface for this purpose, such as Helmholtz resonators,[4] membranes,[5,6] coiled spaces,[7,8] etc. In the above efforts, the soundproof mechanism of the localized resonance or Fano-like interference inevitably induces the narrow band effect. In fact, the noise usually covers multiple discrete characteristic frequencies of noise sources. Thus, some efforts have also been made to broaden the working frequency range of the soundproof barriers with different working mechanisms, such as, double-layered perforated metastructures based on acoustic absorbers with multifrequency resonances,[9] broadband acoustic silencer with ventilation based on slit-type gradient Helmholtz resonators,[10] hornlike helical metasurfaces based on the superposition between monopolar and dipolar resonant modes,[11] 3D soundproof cage structure based on the phononic band gaps,[12] and multiband omnidirectional ventilated acoustic barriers with localized acoustic rainbow trapping metastructures.[13] In fact, it is well known that the thicker metamaterials are required for covering the wider soundproof band. However, the noise usually comes from some specific noise sources with the special eigenfrequency, instead of perfect continuous ones. Thus, a barrier with a customized spectrum to achieve sound insulation at the desired eigenfrequency may be more intelligent and convenient for satisfying the practical applications. Based on this content, a customizable acoustic metamaterial barrier, which is a composite structure consisting of a Helmholtz resonator and a microperforated panel, has been designed to achieve intelligent and selective sound insolation.[14] For practical scenes, it is worth looking forward to the intelligent active soundproof barriers with the advanced advantages of compact volume, tunable working frequency, and low processing cost.

Moreover, a conventional soundproof barrier made with the passive metamaterials usually insulates the sound transmission for both incident directions, that is, reciprocal acoustic insulation. However, in some special application senses, unidirectional

Y. Zhuo, X. Chen, Z. Liu, Z.-Q. Sheng, H.-W. Wu
School of Mechanics and Photoelectric Physics
Anhui University of Science and Technology
Huainan 232001, China
E-mail: chenxue@aust.edu.cn; hwwu@aust.edu.cn
H.-W. Wu
Institute of Energy
Hefei Comprehensive National Science Center (Anhui Energy Laboratory)
Hefei 230031, China

The ORCID identification number(s) for the author(s) of this article can be found under https://doi.org/10.1002/admt.202301693

DOI: 10.1002/admt.202301693

soundproofing is required to insulate the interference from the outside noise signals but permit the communicated signal to pass through (even enhancement) from the inside. Unfortunately, reciprocity is a fundamental property of passive linear wave dynamic systems in the different physical branches, including matter waves, optical waves, acoustic waves, and elastic waves. That is to say, a wave transmitted from source to receiver is symmetric when the source and receiver are switched in their locations. For a long time, breaking the reciprocity is a persistent pursuit for designing the nonreciprocal devices with advantaged properties. In matter-wave system, the nonreciprocity can be easily realized by diodes and transistors in electronic systems by inflicting an external electric field. In optical wave systems, nonreciprocity have been demonstrated by the Faraday effect with magnetic field biasing,[15] nonlinearity,[16,17] topological insulators,[18–20] and systems with angular momentum bias.[21] For acoustic wave system, the nonreciprocity is usually achieved by nonlinear effects that convert the fundamental modes into high harmonics.[22–25] However, acoustic nonlinear effects are weak and demanding for most materials. With the development of acoustic metamaterials, based on the external basis of the constant flow or directional modulation, the sound topological insulators can break the reciprocity to control the acoustic wave directional transmission.[26–29] Furthermore, it is found that tunable prisms and lossy acoustic gradient index metasurfaces can also achieve acoustic asymmetric transmission.[30–31] Very recently, due to the progress in obtaining tunable metamaterial parameters,[32] time-varying material properties have been being added as a new knob in controlling wave using metamaterials.[33–36] In this case, the continuous translational symmetry of metamaterials is broken, and many interesting phenomena have been being proposed and under active exploration, the most prominent one is the magnet-free nonreciprocity.[37–40] In this content, it is significant to design the nonreciprocal soundproof barrier for one-way sound insulation as an alternative strategy in special application senses.

In this paper, we propose a nonreciprocal soundproof barrier made with active nonlocal metastructure (ANM) which constitutes of a pair of spatially separated microphones and a speaker controlled with a microcontroller. In the microcontroller, we use an inverse process to pick the incident noise frequency detected by the microphone, then automatically tune the resonating frequency of the performed Lorentz resonant response to insulate the noise signals. Owing the spatial distance between the microphone and speaker induces the asymmetry for the two incident ends, it will tailor the acoustic wave transmission for realizing unidirectional acoustic insulation. The results by theoretical calculation and experiment measurement indicate that the active acoustic barrier can realize the suppressive effect in one direction and the enhancive effect in the other one for intelligently matching the incident signal. The nonreciprocal level and transmission losses can be freely tuned by tailoring the resonating parameters in the microcontroller and the sound insulation bandwidth can be further widened by constructing multifrequency-ANM. Furthermore, we can also switch the function of the active soundproof barrier to forward, backward, and bidirectional sound insulation by changing the spatial nonlocal distance between the microphone and speaker. Most importantly, our acoustic metastructure can be extended from a one-dimentional waveguide to a two-dimentional plane, which confirms that it is still effective for open-field acoustic environments. The versatile active soundproof barrier with the advantages of frequency-selectable, function-switchable, compact volume, and high ventilation efficiency, may provide alternative strategies to satisfy the requirements of various application scenes.

2. Results and Discussion

2.1. Working Mechanism of the Nonreciprocal Sound Transmission

As a start, we first present an application scenario in **Figure 1a**, where the outdoor noise generated from the car is insulated to keep silence in the room, while the effective signal is desired to enhance from indoors to outdoors. For more clearly show our strategy, Figure 1b is an enlarged view of the window part for the application scenario. The incident noise signal marked by red waveforms is insulated into indoors by the ANM which consists with a pair of spatially separated microphones ("D") and a speaker ("S") controlled by a microcontroller ("MC") as shown as Figure 1b, on the other hand, the communicated signal marked by green waveform from indoors to outdoors is enhanced. To demonstrate the working mechanism of nonreciprocal sound insulation, we set an ANM on a one-dimentional acoustic waveguide manufactured using 3D printing technology, whose transmission channel dimensions are much smaller than the incident signal wavelength. As shown in Figure 1c, there are two speakers labeled with "LS" and "RS" at the left and right ends to generate incident signals. Microphone D and speaker S are inserted through two small holes at the top of the one-dimentional hollow waveguide and do not block the propagation of sound waves. The side view of our test system is shown in the upper right corner of Figure 1c, we can see that there are no obstructions inside the waveguide. The practical ANM have a distance d between the speaker and microphone, then the transmitted and reflected signals are picked up by four detected microphones for obtaining the transmissivity and reflectivity.

In the microcontroller, we perform a convolutional kernel to process the detected signal, which can be expressed as: $\gamma\ (t) = g\sin\left(\omega_{\text{res}}t + \theta\right)\exp\left(-\ \gamma t\right)\Theta(t)$. Here, $g,\ \omega_{\text{res}}, \theta,\ \gamma$ correspond to the resonating strength, resonating angular frequency, line-shape tuning parameter, and decay rate. $\Theta(t)$ is the Heaviside step function for implementing a causal response in the microcontroller. By Fourier transforming the $\gamma\,(t)$ in time, the convolutional kernel in the frequency domain can be approximated as:

$$Y\left(f\right) \cong \frac{g}{2}\left(\frac{e^{i\theta'}}{\omega_{\text{res}} + \omega + i\gamma} + \frac{e^{-i\theta'}}{\omega_{\text{res}} - \omega - i\gamma}\right) \quad (1)$$

where $f = \omega/2\pi$ is the incident frequency, and the line-shape tuning parameter $\theta' = \theta + \delta\theta$, $\delta\theta$ attribute from a fixed time delay for performing program and all electronic components, and θ is a selectable value in the program to control the Lorentz response as passive or active case. For example, for $\theta' = -\pi/2$, the response corresponds to a passive Lorentz resonating shape, and the real and imaginary part of the response $Y(f)/i$ are shown in Figure 1d as red and black lines, where the parameters are selected as $\omega_{\text{res}} = 2\pi \times 1\,kHz$, $g = 2\pi \times 30\ Hz$, $\gamma = 2\pi \times 10\ Hz$. Then, the

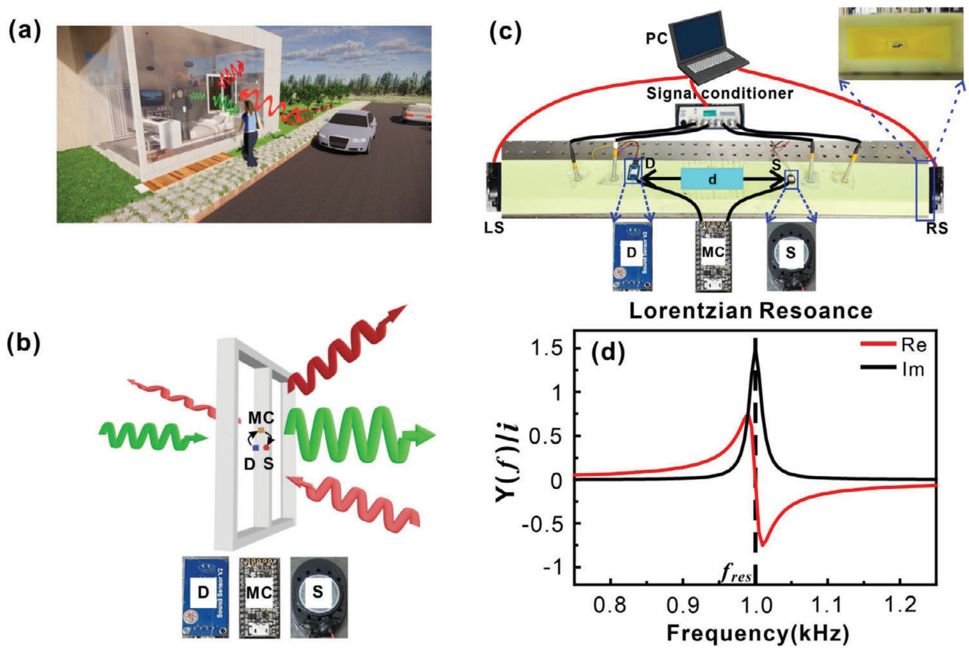

Figure 1. The application scenario and experimental sets. a) The application scenario that require nonreciprocal sound insulation, that is, the noise signal from the car in outdoors is suppressed into the room, while the effective signal from indoors is enhanced and transmitted into outdoors. b) Localized enlarged view of the intelligent soundproof barrier arranged on the window. The noise signal marked by red from the outdoors is mostly reflected back to outside and the green effective signal from indoors is enhanced to outdoors. The three electron components labeled by "D", "MC" and "S" correspond to the microphone, microcontroller, and speaker. c) The experimental sets. The distance between "D" and "S" is set as d, and connected by "MC". LS and RS correspond to the sound sources at the left and right ends, the transmitted and reflected signals are detected by the four microphones. The upper right corner shows the inner of the one-dimentional waveguide loading the ANM. d) The performed convolution kernel in the microcontroller satisfies the Lorentzian resonating shape in the frequency domain, the red and black lines represent the real and imaginary components of the resonating response $Y(f)/i$, respectively.

convolution result $S(f) = Y(f)D(f)$ is feed back to the speaker in generating a resonating scattering waves. For the ANM, the spatial distance d between the microphone and speaker generates asymmetry for the whole system and induces the different transmissivity coefficients at the right and left ends of the waveguide as:

$$t_R(f) = \frac{1 + Y(f)\,e^{-i\phi} - Y(f)\,e^{i\phi}}{1 - Y(f)\,e^{i\phi}} \quad (2)$$

$$t_L(f) = \frac{1 + Y(f)\,e^{i\phi} - Y(f)\,e^{i\phi}}{1 - Y(f)\,e^{i\phi}} \quad (3)$$

The details are given in Note S1 (Supporting Information). The spatial phase is $\phi = kd(k = 2\pi f/c$, $c = 343$ m^{-1}s is the speed of sound in air).

To clear the physical mechanism of the nonreciprocal sound transmission, we define the reference plane as shown in the yellow dashed line in Figure S1 (Supporting Information). For incident wave P_{inL} from the left port of the waveguide, the forward scattering wave (which is defined as the scattering wave direction along the incident direction) have a phase $\psi_R = \mathrm{Arg}(\frac{Y(f)e^{-i\phi}}{1-Y(f)e^{i\phi}})$ comparing with the incident wave p_{inL}, while the phase of the scattering wave becomes as $\psi_L = \mathrm{Arg}(\frac{Y(f)e^{i\phi}}{1-Y(f)e^{i\phi}})$ for the incident wave P_{inR} from the right port. It can be seen from **Figure 2**a1 that the transmissivity ($T = |t|^2$) are overlap for two different incident directions for the spatial distance $d = 0$, that is to say, the sound transmission is reciprocal. The reason of the reciprocal transmission is that the phases of the scattering wave are also overlap as shown in Figure 2a2. To quantify the level of nonreciprocity for two incident directions, we define an isolation factor (IF) as the ratio of the transmissivity $|t_R|^2$ and $|t_L|^2$ as:

$$\mathrm{IF} = \left| 20\mathrm{Log}_{10}\left(\left| t_R(f)/t_L(f) \right| \right) \right| \quad (4)$$

It is obvious that the IF is always 0 for the spatial distance $d = 0$ as shown in Figure 2a3. However, when the spatial distance is set as $d = 0.2\lambda_{res}$ (here $\lambda_{res} = 2\pi c/\omega_{res}$ is the resonating wavelength), we can find that the phase $\psi_R \cong 0$ for the sound propagating from left to right end at the incident frequency $f = 1$ kHz, while the value becomes $|\psi_L| \cong \pi$ for opposite direction. Then, constructive and the destructive interference are presented between the incident wave and scattering wave depending on their phase difference. Thus, the sound transmission is suppressed (enhanced) for the sound propagating from the right (left) to the left (right) port, as shown in Figure 2b1. The similar configuration is used to achieve nonreciprocal transmission[41] by only adding a phase into the scattering wave emitted from speaker as the conventional active noise cancellation. However, in this work, due to the resonating response is performed in microcontroller, and the phase of the scattering wave will be overturned at high frequency as shown as Figure 2b2, the other nonreciprocal transmission at 1.04 kHz can also be found. The sound transmission is

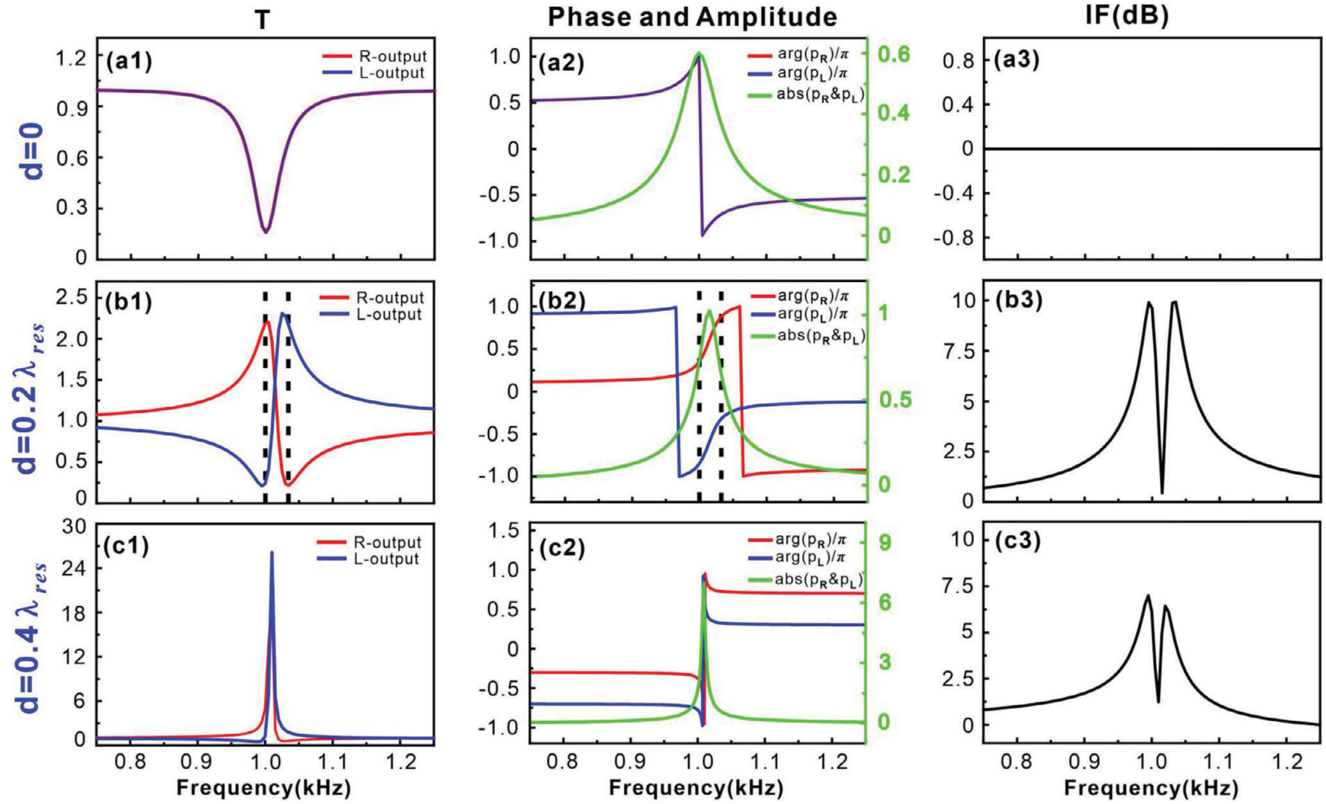

Figure 2. a1–c1) The transmissivity T for different spatial distance $d = 0$, $0.2\lambda_{\mathrm{res}}$, and $0.4\lambda_{\mathrm{res}}$, respectively. The red lines represent the transmissivity for the wave propagating from the left input, and the blue line corresponds to the inverse direction. a2–c2) The phase and amplitude of the scattering waves emitted from the speaker for different spatial distances. a3–c3) Isolation factor for the three spatial distance d, respectively.

enhanced (suppressed) for wave propagating from the right (left) to the left (right) end. Figure 2b3 gives the IF as a function of incident frequency, we can find the two peaks at 1 kHz and 1.04 kHz. As the spatial distance increases to $\mathrm{d} = 0.4\lambda_{\mathrm{res}}$, a very high transmissivity is obtained near the resonance frequency, as shown in Figure 2c1. The state is unstable because of too much sound amplification. Moreover, it can be seen from Figure 2c2 that the phase at the resonance frequency for the sound propagating from left to right is equal to that in the opposite direction, that is, $|\psi_{\mathrm{R}}| \cong |\psi_{\mathrm{L}}|$. And the nonreciprocity is weakened, as shown in Figure 2c3. However, for further increase the distance to $d = 0.8\ \lambda_{\mathrm{res}}$, the nonreciprocity become strong again, but the nonreciprocal characteristic is flipped as shown in Figure S2b1 (Supporting Information). Furthermore, we also calculate the transmissivity for the two incident directions and the IF for different line-shape tuning parameters θ' in Figure S3 (Supporting Information). We can find that the two nonreciprocal transmission (Figure S3a1, Supporting Information) become single stronger nonreciprocal transmission (Figure S3b1, Supporting Information) at resonating frequency due to the $\psi_{\mathrm{R}} \cong 0$ and $|\psi_L| \cong \pi$ occur at the resonating position with the biggest amplitude. It is easy to tune the IF by change the line-shape tuning parameter θ' in our experiment. In following applications of nonreciprocal sound insulation, the value of θ' was set as zero for obtaining stronger nonreciprocal transmission. In this work, the nonreciprocal level and the working frequency can be freely tailored by tuning multiple resonating parameters (resonating strength, resonating frequency, decay rate and line-shape tuning parameter), which will provide a versatile platform to control the nonreciprocal transmission. The details of the simulation model are in Note S4 (Supporting Information).

2.2. Nonreciprocal Soundproof with Nonlocal Acoustic Barrier

In the above section, we have discussed the nonreciprocal mechanism for the acoustic transmission by the ANM in which performed a resonating response. Next, we will use this configuration to investigate the transmission losses for the incident signals propagating along different directions.

To demonstrate the unidirectional soundproof barrier with our configuration, in **Figure 3a**, we give the transmission spectrum for inputting from left and right ports as the red and blue lines (symbols), the lines correspond to the simulated results and the symbols are experimental results. The parameters of the resonating response are selected as $\omega_{\mathrm{res}} = 2\pi \times 1\ kHz$, $g = 2\pi \times 30\ Hz$, $\gamma = 2\pi \times 10\ Hz$ and $\theta' = 0$ in experiment. We can find that the signal is enhanced from left to right port with transmissivity $\mathrm{T} = 2.6$, while it is suppressed along the inverse direction with $\mathrm{T} = 0.15$ at $f = 1$ kHz. To intuitively observe the nonreciprocal level between the two propagated directions, we also give the IF in Figure 3b according to Equation (3), the experimental result agrees well with the simulated result that the maximal IF at 1 kHz as IF = 12 dB. To demonstrate the uni-

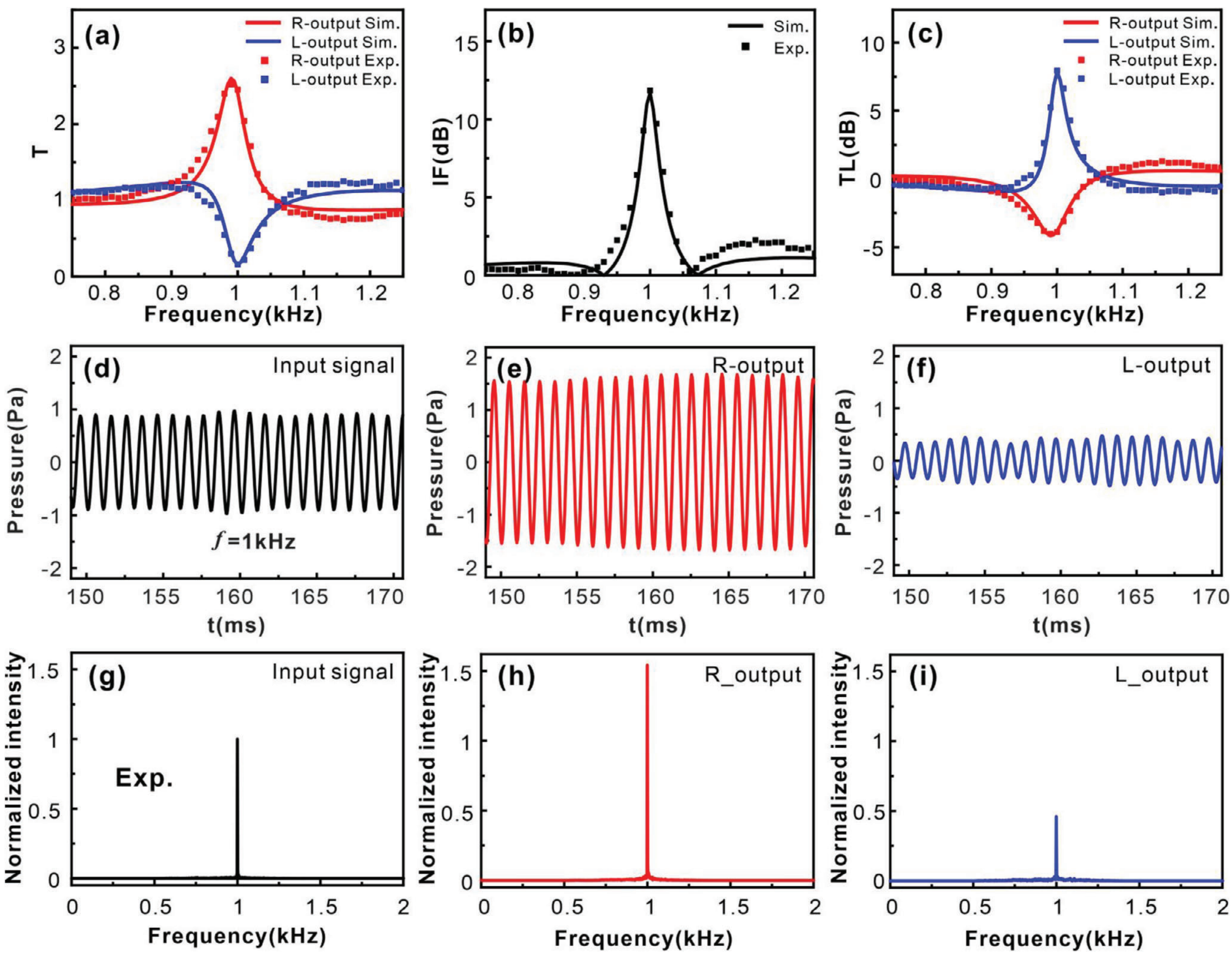

Figure 3. a) The transmissivity for different propagating directions with the parameters: $\omega_{res} = 2\pi \times 1\ kHz$, $g = 2\pi \times 30\ Hz$, $\gamma = 2\pi \times 10\ Hz$ and $\theta' = 0$, the lines and symbols corresponding to simulation and experiment. The distance between D and S is $d = 0.2\lambda_{res}$. b,c) corresponding to the IF and TL. d,e) show the input signal with $f = 1$ kHz and the output signal from the left and right port in the time domain, respectively. g)-i) The experimental results of an input signal with $f = 1$ kHz and output signal from the left and right port in the frequency domain, respectively.

directional sound insulation, we also calculate and measure the transmission losses (TL) in Figure 3c, which can be expressed as:

$$TL = -20\ Log_{10} \left| t\left(f\right) \right| \tag{5}$$

here, the $t(f)$ is transmissivity coefficient. It is not difficult to see that the left output signal is insulated with TL = 8.5 dB, and the right output one is enhanced with TL = −4 dB at 1 kHz. For clearly show the directional soundproof function, we also experimental measure the signal in the time domain as shown in Figures 3d–f and in the frequency domain as shown in Figures 3g–i. The corresponding simulated results in the frequency domain are given in Figure S5 (Supporting Information). Comparing the input signal with frequency $f = 1$ kHz, the right output signal is much stronger than the signal output from the left port. In our configuration, the signal enhanced and suppressed level can be furtherly strengthened by increasing the resonating strength from $g = 2\pi \times 30$ Hz to $2\pi \times 60$ Hz as shown in Figure S6 (Supporting Information) of Supplementary Materials. To illustrate the convenient tuning the soundproof frequency, we also calculate and measure the transmissivity, IF, and TL for different resonating frequencies $f_{res} = 0.95$ kHz, 1.0 kHz, and 1.05 kHz in Figure S7 (Supporting Information). The results show that the nonreciprocal soundproof frequency can be freely tailored by tuning the resonating frequency in the microcontroller. Furthermore, broadband sound insulation can be realized by adding several speakers ("S") in the ANM to construct multifrequency-ANM, as shown in Note S8 (Supporting Information).

In the above example, we have demonstrated that the barrier can insulate the signal in an incident direction, while enhancing the communicated signal in the other incident direction. It is well known that different noise sources will have different eigenfrequencies. Thus, it is significant for automatically adjusting the working frequency of the soundproof barrier according to the incident signals. For achieving the automatic adjustment, we add an extra microcontroller (MC1) to process the probed signal from

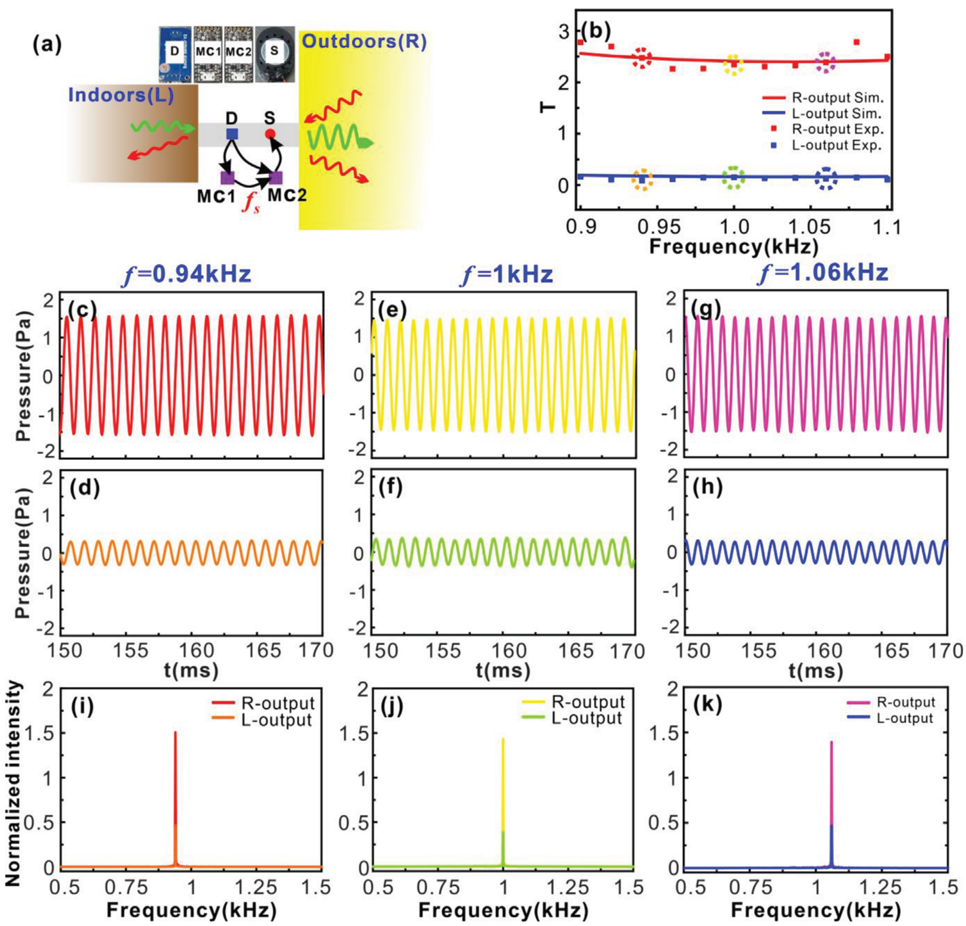

Figure 4. a) shows a diagram of the example scenario, an ANM together with an extra microcontroller (MC1) for detecting the signal frequency f_s to realize nonreciprocal sound insulation that insulates the red noise signal and enhances the green communicated signal incident from outdoors and indoors. b) shows the transmissivity T for continuously changing the incident frequency from 0.9 to 1.1 kHz with different inputting ports, the lines, and symbols corresponding to simulated and experimented results. c) and d,e) and f,g) and h) are the time-domain outputting signals received at the right and left port for different incident signal frequencies $f = 0.94,\ 1.0$ and 1.06 kHz, which is marked in b) with colorful circles. i–k) are the corresponding frequency domain spectra.

the microphone (D) by performing a fast Fourier transform to obtain the incident signal frequency f_s, which can determine the working frequency (resonating frequency f_{res}) in MC2 as shown in Figure 4a. The parameters setting of MC2 are consistent with the legend in Figure 3a, except for the resonance frequency f_{res}. Based on the configuration of the ANM with an extra microcontroller, we want to

realize the intelligent unidirectional sound insulation that the left inputted signal marked by green line is enhanced to outdoors and the right inputting signal with the red line is forbidden into indoors. In **Figure** 4b, we numerically simulate and experimentally measure the transmissivity for continuously changing the incident frequency from 0.9 to 1.1 kHz. The red line and red symbols are the transmissivity by simulation and measurement for input from the left port and output from the right port. The blue line and blue symbols are the transmissivity for inverse incident direction. We can find that the barrier can automatically adjust the working frequency to insulate the signal with different frequencies inputting from the right port and induce low T. In the other direction, the signal can be enhanced as shown in the red line and symbols for different signal frequencies. For clear observation, we give the transmitted signals in time from 150 to 170 ms received at the right port and left port corresponding to Figures 4c–h for the incident wave with different frequencies $f = 0.94,\ 1,\ 1.06$ kHz marked in Figure 4b with dashed circles with different colors. Comparing the outputted signals from right and left port, we can find that the enhanced signal magnitude can arrive at 1.5 Pa, while the suppressed signal magnitude only have 0.4 Pa. The results of the outputted signals in the frequency domain also show that the enhanced signals are achieved inputting from the left port, while the suppressed signals are obtained for the opposite direction, as shown in Figure 4i–k. In fact, the signal strengths can be further enhanced or suppressed for the two incident directions by increasing the resonating strength g as demonstrated in Figure S6 (Supporting Information). Here, we define this unidirectional nonreciprocal sound insulation as backward sound insulation with the nonlocal spatial distance $d = 0.2\ \lambda_{res}$. Furthermore, in Figure 2, we have illustrated that the nonreciprocal sound transmission comes from the spatial nonlocal response of the ANM, that is, the spatial distance

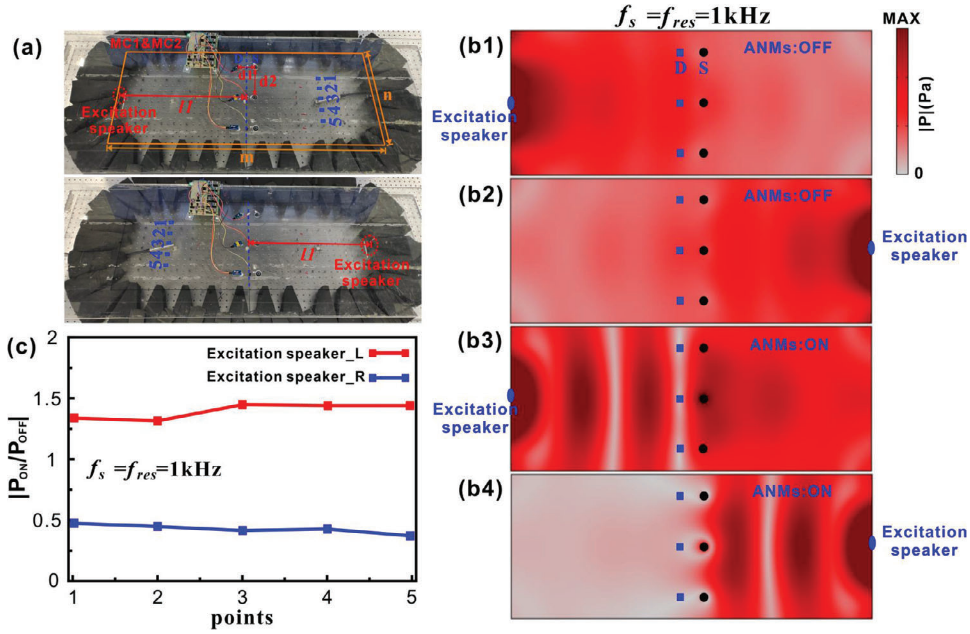

Figure 5. a) Diagrams of the two-dimentional ANMs devices. The top and bottom pictures show the schematic with the excitation source placed on the left or right, respectively. Microphones (D) and speakers (S) are located on either side of the plane midline (blue dash line). The five blue points are the test locations during the experiment. b1,b2) The simulated results of the sound pressure intensity when the ANMs are turned off. b3,b4) The simulated results of the sound pressure intensity when the ANMs are turned on from the left and right ports, respectively. c) The experimental results of the sound pressure intensity ratio ($|P_{ON}/P_{OFF}|$) at the corresponding five blue points.

between the microphone and speaker. Further, we also demonstrate that the spatial distance is tailored from $d = 0.2\ \lambda_{res}$ to 0 and $-0.2\ \lambda_{res}$, the nonreciprocal property of the soundproof barrier can be tuned as shown in Figures S9 and S10 (Supporting Information) to achieve bidirectional and forward sound insulation for satisfying different application senses. These results indicate that our nonreciprocal configuration will provide a versatile platform to control the nonreciprocal transmission.

This acoustic metastructure was extended from a one-dimentional waveguide to a two-dimentional plane to illustrate that it is still valid in an open-field environment. **Figure** 5a shows the device diagram of the ANMs, where the upper and lower acrylic plates are used to simulate a two-dimentional scenario. Sound reflection at the boundaries is reduced by using black angular sound-absorbing foams around the perimeter. The top and bottom pictures in Figure 5a show the schematic with the excitation source placed on the left or right, respectively. The length (m) and width (n) of the two-dimentional plane are 100 and 40cm, respectively. Microphones (D) and speakers (S) are located on either side of the plane midline (blue dash line) and the distance between them is $d1 = 0.2\ \lambda_{res} = 6.86$ cm. The distance between adjacent speakers/microphones (S/D) is $d2 = 14$ cm and $l1 = \frac{m}{2} = 50$ cm represents the distance from the excitation speaker to the plane midline. The five blue points are the test location during the experiment and the incident frequency is set to the resonance frequency ($f_s = f_{res} = 1$ kHz). The simulated results of the sound pressure intensity are

shown in Figure 5b1,2 when the ANMs are turned off. It can be seen that the sound pressure intensity is reduced regardless of the location of the excitation source. Figure 5b3,4 shows the simulated results when the ANMs are turned on. It is clear that the sound pressure intensity in the right region is enhanced when the excitation speaker is placed on the left side, while the sound pressure intensity in the left region is weakened when the excitation speaker is placed on the right side. The experimental results of the sound pressure intensity ratio ($|P_{ON}/P_{OFF}|$) at the corresponding five blue points are presented in Figure 5c. The ratio is ≈1.4 (red line) when the excitation speaker is placed on the left side, while the ratio is ≈0.45 (blue line) when the excitation speaker is placed on the right side. Therefore, it can be concluded that the ANMs still exhibit nonreciprocal transmission in the two-dimentional plane. The corresponding movie of their actual testing results is shown in Note S12 and Movie S1 (Supporting Information) to interpret this exotic physical phenomenon intuitively. Finally, as shown in Note S11 (Supporting Information), we have also confirmed that the ANMs can maintain the nonreciprocal property under different incidence directions and it is highly adaptable to the environment.

3. Conclusion

In conclusion, we have proposed an active nonlocal acoustic metastructure, which includes a pair of spatially separated microphones and a speaker connected by a microcontroller that performed a convolution kernel of Lorentz-shape resonating response, to realize nonreciprocal sound insulation. By theoretical analysis, we find that the nonreciprocal sound transmission comes from an asymmetric phase of the scattering waves induced by the spatial distance for the two incident directions. Particularly, we can freely tune the unidirectional soundproof strength, nonreciprocal level, and working frequency by adjusting the parameters of the resonating response in the microcontroller. Based on the advantage of multiple parameters tunable, we add an extra microcontroller to detect the incident signal frequency to determine the working frequency of the ANM for realizing the nonreciprocal sound insulation automatically. Furthermore, this acoustic metastructure was extended from a one-dimentional waveguide to a two-dimentional plane to illustrate that it is still valid in an open-field environment. Our experimentally measured results demonstrate the theoretical prediction that the configuration of the ANM can insulate the noise signal propagating along a direction and enhance the communicated signal along the other propagated direction. The nonreciprocal soundproof barrier for unidirectional sound insulation can provide an alternative strategy in special application senses.

4. Experimental Section

All experiments were conducted in a one-dimentional waveguide or two-dimentional plane made of acrylic, which featured an ANM placed on top of it with a spatial distance of d, as depicted in Figures 1, 5. In the ANM, a pair of speakers and a microphone connect with a microcontroller (Adafruit ItsyBitsy M4 Express). The total delay time for the ANM, comprising of the delay time for the microphone, speaker, and electronic delay for the microcontroller, was experimentally obtained to be $\delta t = 420$ µs ≈ 1 kHz (the center frequency of our interested range). To achieve a Lorentz resonant response with a digital microcontroller, the equation: $\partial_t^2 S(x_S, t) + 2\gamma\partial_t S(x_S, t) + \omega_{res}^2 S(x_S, t) = -g\partial_t D(x_D, t)$ was transformed into a time-discrete model but with the frequency response function Y now approximated as the open-circuit frequency response function connecting D to S to be implemented electronically. Here, the $S(x_S,t)$ is the signal emitted by speaker with the position x_S, $D(x_D,t)$ is the signal detected by microphone with the position x_D. The sampling frequency was set at 57.6 kHz, with a sampling period of 17.36 µs. Additionally, the program for the Lorentz response was designed to finish within one sampling period in preparation for the next sample to be sent to the speaker. The time delay, as well as the frequency dispersive response for the speakers and microphones, were compensated (around the center frequency 1 kHz) by additional digital filters in the microcontroller. The four-point measurement method is utilized in conjunction with a National Instruments DAQ device to determine the reflection and transmission signals. Through the application of the Fourier transform, the transmission ($t(f)$) and reflection coefficients ($r(f)$) are obtained in all figures.

In the simulation part, we use finite-element simulations performed with the time-domain module of pressure acoustics in the commercial software of Comsol Multiphysics. We investigate the nonreciprocal transmission of the ANM for air-borne acoustics. The metastructure is constructed using a pair of nonlocal microphones and a speaker in a one-dimentional waveguide, which is modeled as a point source in its secondary radiation in the waveguide. The secondary radiation of the point sources is governed by

$$\partial_x p\,(x, t) + \rho_0 \partial_t \nu\ \ (x, t) = 0 \tag{6}$$

$$\partial_x \nu\,(x, t) + \beta_0 \partial_t p\ \ (x, t) = \Sigma_i \delta\,(x - x_S)\,\frac{2}{\rho_0 c} S\,(x_S, t) \tag{7}$$

where $c = 1/\sqrt{\beta_0 \rho_0}$ is air sound speed, ρ_0 is the density of air and β_0 is the compressibility of air. The right-hand term of the equation represents the monopolar secondary point sources generated by speakers (S) at positions x_S. The Lorentzian model is implemented by an ordinary differential equations (ODE) module, which responds to the pressure field by

$$\partial_t^2 S\,(x_S, t) + 2\gamma\partial_t S\,(x_S, t) + \omega_{res}^2 S\,(x_S, t) \ = \ -g\partial_t D\,(x_D, t) \tag{8}$$

where ω_{res} is the resonating (radial) frequency, γ is the resonating linewidth, and g is the resonance strength. The $D(x_D,t)$ is the total pressure field picked by the microphone which includes the incident field and the secondary radiation fields from the speakers. The nonlocal spatial distance $d = x_S - x_D$. Four microphones are placed at the two ends of one-dimentional waveguide for receiving the time-domain signals, using the Fourier transform, the transmission ($t(f)$) and reflection coefficients ($r(f)$) can be obtained in all figures.

Supporting Information

Supporting Information is available from the Wiley Online Library or from the author.

Acknowledgements

The authors acknowledge support from the Major Scientific Research Projects of Colleges and Universities in Anhui Province (grant no. 2022AH040114); the University Synergy Innovation Program of Anhui Province (grant no. GXXT-2022-015); the Natural Science Research Project of Anhui Educational Committee (grant no. 2022AH050850) and the Scientific Research Foundation for High-level Talents of Anhui University of Science and Technology (grant no. 2021yjrc24).

Conflict of Interest

The authors declare no conflict of interest.

Author Contributions

H.W.W. conceived the idea and designed the experiment. Y.Z. and Z.L. prepared the samples and performed the experiments. Y.Z. and X.C. conducted the numerical simulations. Y.Z., X.C., Z.Q.S., and H.W.W. contributed to the writing of the paper. X.C., Z.Q.S., and H.W.W. supervised the entire study.

Data Availability Statement

The data that support the findings of this study are available from the corresponding author upon reasonable request.

Keywords

acoustic insulation, acoustic metamaterials, active controller, nonreciprocal sound transmission

Received: October 6, 2023
Revised: December 1, 2023
Published online:

[1] J. Kang, M. W. Brocklesby, *Appl. Acoust.* **2005**, *66*, 669.
[2] X. Yu, S. K. Lau, L. Cheng, F. Cui, *Appl. Acoust.* **2017**, *117*, 113.
[3] S. Kumar, H. P. Lee, *Crystals* **2020**, *10*, 686.
[4] S. H. Kim, S. H. Lee, *AIP Adv.* **2014**, *4*, 117123.
[5] Z. Yang, H. M. Dai, N. H. Chan, G. C. Ma, P. Sheng, *Appl. Phys. Lett.* **2010**, *96*, 041906.
[6] G. Ma, M. Yang, S. Xiao, Z. Yang, P. Sheng, *Nat. Mater.* **2014**, *13*, 873.
[7] Y. Cheng, C. Zhou, B. G. Yuan, D. J. Wu, Q. Wei, X. J. Liu, *Nat. Mater.* **2015**, *14*, 1013.
[8] X. Su, D. Banerjee, *Phys. Rev. Appl.* **2020**, *13*, 064047.

[9] L. J. Li, B. Zheng, L. M. Zhong, J. Yang, B. Liang, J. C. Cheng, *Appl. Phys. Lett.* **2018**, *113*, 103501.
[10] H. Nguyen, Q. Wu, X. C. Xu, H. Chen, S. Tracy, G. L. Huang, *Appl. Phys. Lett.* **2020**, *117*, 134103.
[11] M. Sun, X. S. Fang, D. X. Mao, X. Wang, Y. Li, *Phys. Rev. Appl.* **2020**, *13*, 044028.
[12] C. Liu, H. Wang, B. Liang, J. Chen, Y. Lai, *Appl. Phys. Lett.* **2022**, *120*, 231702.
[13] H. W. Wu, Y. Q. Yin, Z. Q. Sheng, Y. Li, D. X. Qi, R. W. Peng, *Phys. Rev. Appl.* **2021**, *15*, 054033.
[14] Z. H. Su, H. Luo, S. Y. Gao, Z. T. Luo, Y. F. Zhu, H. Zhang, *Phys. Rev. Appl.* **2022**, *18*, 064029.
[15] J. D. Adam, L. E. Davis, G. F. Dionne, E. F. Schloemann, S. N. Stitzer, *IEEE Trans. Microwave Theory Tech.* **2002**, *50*, 721.
[16] D. L. Sounas, A. Alù, *Phys. Rev. Lett.* **2017**, *118*, 154302.
[17] D. L. Sounas, J. Soric, A. Alù, *Nat. Electron.* **2018**, *1*, 113.
[18] M. C. Rechtsman, J. M. Zeuner, Y. Plotnik, Y. Lumer, D. Podolsky, F. Dreisow, S. Nolte, M. Segev, A. Szameit, *Nature* **2013**, *496*, 196.
[19] L. Lu, J. D. Joannopoulos, M. Soljačić, *Nat. Photon.* **2014**, *8*, 821.
[20] A. B. Khanikaev, G. Shvets, *Nat. Photon.* **2017**, *11*, 763.
[21] D. L. Sounas, C. Caloz, A. Alù, *Nat. Commun.* **2013**, *4*, 2407.
[22] B. Liang, B. Yuan, J. C. Cheng, *Phys. Rev. Lett.* **2009**, *103*, 104301.
[23] B. Liang, X. S. Guo, J. Tu, D. Zhang, J. C. Cheng, *Nat. Mater.* **2010**, *9*, 989.
[24] N. Boechler, G. Theocharis, C. Daraio, *Nat. Mater.* **2011**, *10*, 665.
[25] B. I. Popa, S. A. Cummer, *Nat. Commun.* **2014**, *5*, 3398.
[26] Z. Yang, F. Gao, X. Shi, X. Lin, Z. Gao, Y. Chong, B. Zhang, *Phys. Rev. Lett.* **2015**, *114*, 114301.
[27] X. Ni, C. He, X. C. Sun, X. P. Liu, M. H. Lu, L. Feng, Y. F. Chen, *New J. Phys.* **2015**, *17*, 053016.
[28] R. Fleury, A. B. Khanikaev, A. Alù, *Nat. Commun.* **2016**, *7*, 11744.
[29] Y. Ding, Y. Peng, Y. Zhu, X. Fan, J. Yang, B. Liang, X. Zhu, X. Wan, J. Cheng, *Phys. Rev. Lett.* **2019**, *122*, 014302.
[30] Z. Zhang, L. Bai, L. Xu, W. X. Jiang, T. J. Cui, *Phys. Status Solidi RRL* **2021**, *15*, 2100163.
[31] Y. Li, C. Shen, Y. B. Xie, J. F. Li, W. Q. Wang, S. A. Cummer, Y. Jing, *Phys. Rev. Lett.* **2017**, *119*, 035501.
[32] H. T. Chen, W. J. Padilla, J. M. Zide, A. C. Gossard, A. J. Taylor, R. D. Averitt, *Nature* **2006**, *444*, 597.
[33] A. Rogov, E. Narimanov, *ACS Photonics* **2018**, *5*, 2868.
[34] P. A. Huidobro, E. Galiffi, S. Guenneau, R. V. Craster, J. B. Pendry, *Appl. Phys. Sci.* **2019**, *116*, 24943.
[35] Y. Hadad, D. L. Sounas, A. Alù, *Phys. Rev. B* **2015**, *92*, 100304.
[36] C. Caloz, Z. L. Deck-Léger, *IEEE Trans. Antennas Propag.* **2019**, *68*, 1569.
[37] Y. Wang, B. Yousefzadeh, H. Chen, H. Nassar, G. Huang, C. Daraio, *Phys. Rev. Lett.* **2018**, *121*, 194301.
[38] J. W. Zang, D. Correas-Serrano, J. T. S. Do, X. Liu, A. Alvarez-Melcon, J. S. Gomez-Diaz, *Phys. Rev. Appl.* **2019**, *11*, 054054.
[39] S. Taravati, *Phys. Rev. Appl.* **2018**, *9*, 064012.
[40] J. Marconi, E. Riva, M. Di Ronco, G. Cazzulani, F. Braghin, M. Ruzzene, *Phys. Rev. Appl.* **2020**, *13*, 031001.
[41] N. Geib, A. Sasmal, Z. Z. Wang, Y. X. Zhai, B. I. Popa, K. Grosh, *Phys. Rev. B* **2021**, *103*, 165427.

